2026 American Control Conference

Multi-agent UAV navigation using a Particle Filter driven by magnetic anomaly gradients

Dominik Pisarski, **Rami Faraj**, Łukasz Jankowski
Institute of Fundamental Technological Research, Polish Academy of Sciences

Summary. This work presents a magnetic anomaly-based localization method for UAVs operating in GNSS-denied environments using a collaborative multi-agent approach that integrates magnetic and inter-UAV distance measurements within a Particle Filter framework via Bayesian inference. The method leverages inter-UAV ranging through ad hoc communications, making it well-suited for dynamic formations and resilient to communication disruptions and UAV failures. Following an introduction to the multi-agent mission problem and a formal description of the proposed Distributed Particle Filter algorithm, a case study is presented using a magnetic field map and flight logs collected experimentally with a dedicated VTOL platform equipped with a high-precision scalar magnetometer operating over the Baltic Sea. Evaluation of various collaborative scenarios demonstrates that incorporating inter-UAV ranging significantly improves localization accuracy, reducing positioning error by 71-78% across different collaboration strategies compared to the non-collaborative baseline.

COLLABORATIVE PARTICLE FILTER FOR UAV FORMATIONS

We consider a group of N UAV agents that communicate via channels defined by a graph topology *T* (see Fig. 1). Let $g_t^{ij} \in \{0,1\}$ be a binary variable such that $g_t^{ij} = 1$ if a bidirectional communication link exists between agents *i* and *j* at time *t*, and otherwise. The set of agents communicating with agent *i* at time step *t* is given by:

$$\mathcal{G}_t^i = \left\{ j \,\middle|\, g_t^{ij} = 1,\ j \in \{1, 2, \ldots, N\} \right\}. \tag{1}$$

Communication is used to estimate inter-agent distances via Ultra-Wideband (UWB) protocols. These distance measurements, along with magnetic measurements, are then fused within a particle filter to estimate the position of each agent. The particle filter algorithm proceeds as follows:

Step A: Calculation of the particles' weights/estimation of UAV positions. Assuming the fusion of magnetic field measurement and inter-agent distance, the posterior distribution of the location of the local *i*th UAV is as follows:

$$p\left(\mathbf{x}_t^i \,\middle|\, M_t^i = m_t^i \wedge D_t^{ij} = d_t^{ij}, j \in \mathcal{G}_t^i \right) \approx \sum_{k=1}^{N_t^i} w_t^{k,i}\, \delta(\mathbf{x}_t^i - \mathbf{x}_t^{k,i}). \tag{2}$$

The weights $w_t^{k,i}$ are computed using the probability density of the magnetic field measurement, along with the probability density of the inter-agent distances:

$$w_t^{k,i} \propto p\left(m_t^i \,\middle|\, X_t^i = \mathbf{x}_t^{k,i}\right) \prod_{j \in \mathcal{G}_t^i} \sum_{l=1}^{N_t^j} p\left(d_t^{ij} \,\middle|\, X_t^i = \mathbf{x}_t^{k,i} \wedge X_t^j = \mathbf{x}_t^{l,j}\right). \tag{3}$$

The measurement probability densities in Eq. (3) are determined by the Gaussian character of the measurement errors $p(m_t^i | X_t^i = \mathbf{x}_t^{k,i})$ while the probability density of the inter-agent distance is:

$$p\left(d_t^{ij} \,\middle|\, X_t^i = \mathbf{x}_t^{k,i} \wedge X_t^j = \mathbf{x}_t^{l,j}\right) = \frac{1}{\sigma_{\mathrm{D}}\sqrt{2\pi}} \exp\left(-\frac{1}{2}\left(\frac{d_t^{ij} - \|\mathbf{x}_t^{k,i} - \mathbf{x}_t^{l,j}\|}{\sigma_{\mathrm{D}}}\right)^2\right). \tag{4}$$

The mean of the posterior distribution Eq. (2) is the estimated position $\bar{\mathbf{x}}_t^i$ of the *i*th UAV. Given the normalized weights, it equals:

$$\bar{\mathbf{x}}_t^i = \sum_{k=1}^{N_t^i} w_t^{k,i}\, \mathbf{x}_t^{k,i}. \tag{5}$$

Step B: Resampling of particles. Given the particles and their weights, a new set of particles is generated for the next time step *t* + 1. This involves discarding the lowest-weight particles and generating new particles by sampling from a certain continuous approximation to the empirical distribution of the retained ones.

Step C: Propagation of particles. Particle locations are updated using the assumed propagation model:

$$\mathbf{x}_{t+1}^{k,i} \longleftarrow \mathbf{x}_t^{k,i} + \Delta\mathbf{x}_t^i, \qquad k = 1, 2, \ldots, N_{t+1}^i, \tag{6}$$

where $\Delta\mathbf{x}_t^i$ is the propagation increment between time step t and t + 1, which is estimated using appropriate onboard instruments.

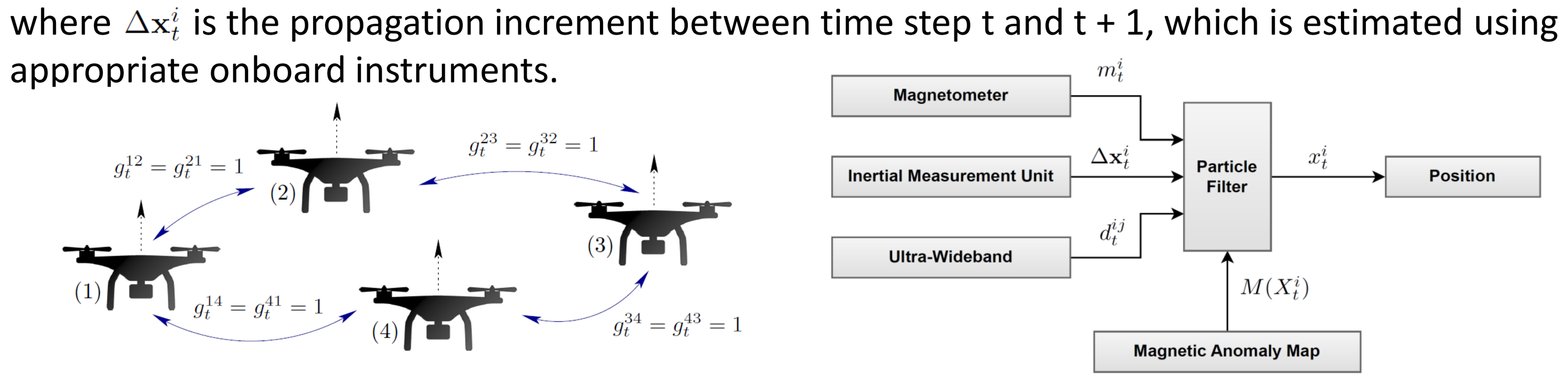

Fig. 1. Example of communication topology (represented by the blue arrowed graph, l.h.s.); instrumentation scheme for the developed Particle Filter (r.h.s.).

CASE STUDY

The developed algorithm was validated using a custom designed platform: a 22 kg VTOL (Vertical Take-Off and Landing) aircraft with a 3.5 m wingspan, equipped with a tail-mounted magnetic measurement system (see Fig. 2) that employed high-precision cesium scalar magnetometers. During the initial calibration, the magnetic system was adjusted to compensate for orientation-induced disturbances. First, ground-based measurements were performed using a specially designed non-magnetic tripod to acquire calibration data. Next, a neural network was trained to model the relationship between magnetic disturbances and aircraft attitude (yaw, pitch, and roll angles). Output of the trained model was subtracted from the measured magnetic field to compensate for attitude-dependent disturbances. The calibrated magnetometer system was deployed to map the magnetic field over a sector of the Baltic Sea region, spanning longitudes 16.650–16.685° and latitudes 54.574–54.590°, see Fig. 3. The map was generated from the collected data using Gaussian process regression.

To evaluate the distributed localization algorithm (Table 2), the described custom UAV platform was deployed to collect magnetic field data along a curved trajectory (from 16.670 ° E, 54.582 ° N to 16.671° E, 54.585° N) within the mapped region. Fig. 3 l.h.s. illustrates the flight path, while r.h.s. provides the geographical context. Given the availability of only a single instrumented UAV, the formation flight of three agents is simulated using the acquired data. The simulated formation is sequenced as follows: agent (3) leads, followed by agent (2), and then agent (1).

Fig. 2. Calibration stand for the tail-mounted scalar magnetometer. The stand enables systematic data collection across the UAV's operational attitude range while maintaining the magnetometer in a fixed position, which isolates it from local magnetic anomalies (l.h.s.), VTOL platform with a tail-mounted magnetometer for magnetic field mapping and formation-flight data simulation (r.h.s.).

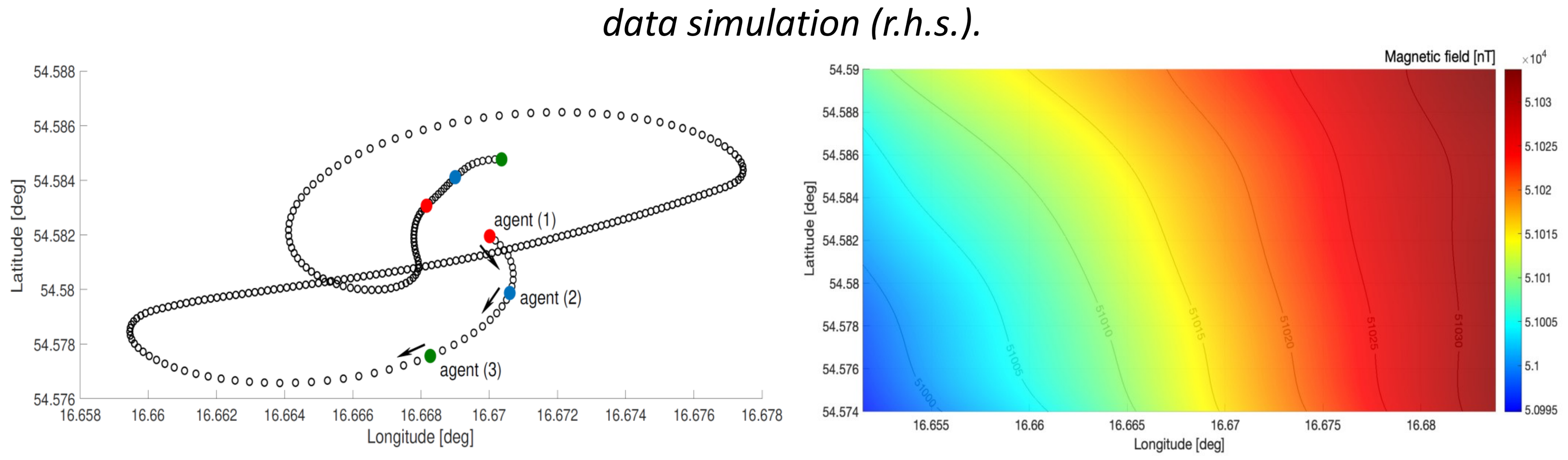

Fig. 3. Visualization of UAV agents' flight trajectories with departure and destination markers (l.h.s.), Geomagnetic map derived from field measurements, covering approximately 3×2 km of coastal terrain along the Baltic Sea (r.h.s.).

RESULTS

To evaluate the effectiveness of the proposed method, 1000 simulations were performed for three different collaboration topologies, which relate to full communication T^1, linear T^2 and leader-follower structure T^3, respectively. Below exemplary result for full inter-agent communication is shown, see Fig. 4. The position error (blue curve), averaged over 1000 runs and summed across the three agents, shows a relatively high initial error in the Particle Filter estimates (83.1 [m]), which results from the random initialization of the particles over a relatively large radius. The mean total position error remains below 53.3 [m], with a final total error of 31.9 [m] (both values summed across all agents). The per-agent mean position errors are consistent, ranging from 9.0 [m] for agent (3) to 10.8 [m] for agent (1). Compared to the non-collaborative baseline T^0, the overall mean position error is reduced by 77.9%.

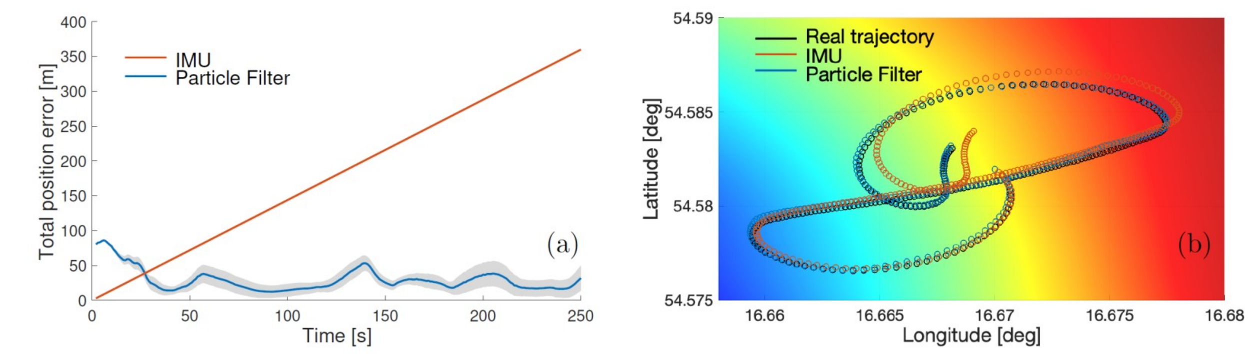

Fig. 4. Comparison of PF performance depending on the velocity estimation method for lack of initial error (l.h.s) and initial error of 100 mm (r.h.s.) – full communication topology T^1.

Tab. 1. Localization errors under different inter-agent distance information topologies: mean ± standard deviation over 1000 trials, averaged over the considered flight time [m].

	Non-collaborative $\mathcal{T}^0$ mean/std	Collaborative $\mathcal{T}^1$ mean/std	Collaborative $\mathcal{T}^2$ mean/std	Collaborative $\mathcal{T}^3$ mean/std
Agent (1)	45.84/14.29	10.82/4.11	12.91/4.72	12.94/4.48
Agent (2)	44.18/14.35	9.17/3.90	11.67/4.67	13.11/5.17
Agent (3)	41.03/14.50	9.01/4.06	11.98/5.18	11.85/4.97
Total (1)–(3)	131.05/24.76	29.00/10.48	36.56/12.88	37.90/12.78

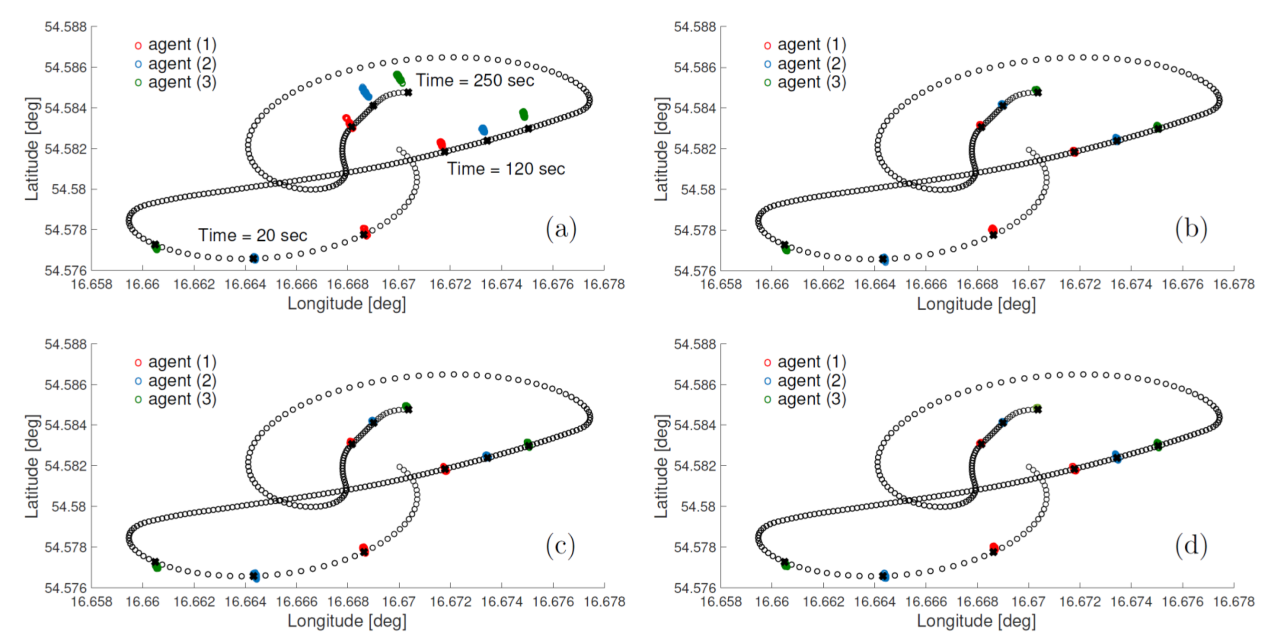

Fig. 5. Comparison of particle distributions at t =20,120, and 250 [s] for the communication topologies T^0(a), T^1(b), T^2(c), and T^3(d). The reference trajectory is shown in the background; black crosses mark the true positions at the sampled times. The results are from a single representative simulation out of 1000 runs.

Acknowledgement. The support of the National Centre for Research and Development (NCBiR) granted through the agreement DOB-SZAFIR/01/B/018/04/2021 is gratefully acknowledged.

May 26-29, 2026 | New Orleans, Louisiana